

Review

Chemocatalytic Conversion of Lignocellulosic Biomass to Ethanol: A Mini-Review

Zhenggang Gong [†] , Xianqing Lv [†], Junhui Yang, Xiaolin Luo ^{*} and Li Shuai ^{*}

College of Materials Engineering, Fujian Agriculture and Forestry University, Fuzhou 350002, China

^{*} Correspondence: xluo53@163.com (X.L.); lishuai@fafu.edu.cn (L.S.)[†] These authors contributed equally to this work.

Abstract: Ethanol has been widely used as a clean fuel, solvent, and hydrogen carrier. Currently, ethanol is generally produced through fermentation of starch- and sugarcane-derived sugars (e.g., glucose and sucrose) or ethylene hydration. Its production from abundant and inexpensive lignocellulosic biomass would facilitate the development of green and sustainable society. Biomass-derived carbohydrates and syngas can serve as important feedstocks for ethanol synthesis via biological and chemical pathways. Nevertheless, the biological pathway for producing ethanol through biomass-derived glucose fermentation has the disadvantages of long production period and carbon loss. These issues can be effectively mitigated by chemocatalytic methods, which can readily convert biomass to ethanol in high yields and high atomic efficiency. In this article, we review the recent advances in chemocatalytic conversion of lignocellulosic biomass to ethanol, with a focus on analyzing the mechanism of chemocatalytic pathways and discussing the issues related to these methods. We hope this mini-review can provide new insights into the development of direct ethanol synthesis from renewable lignocellulosic biomass.

Keywords: biomass; cellulose; ethanol; chemocatalytic conversion

Citation: Gong, Z.; Lv, X.; Yang, J.; Luo, X.; Shuai, L. Chemocatalytic Conversion of Lignocellulosic Biomass to Ethanol: A Mini-Review. *Catalysts* **2022**, *12*, 922. <https://doi.org/10.3390/catal12080922>

Academic Editor:
Francesco Mauriello

Received: 30 June 2022

Accepted: 19 August 2022

Published: 21 August 2022

Publisher's Note: MDPI stays neutral with regard to jurisdictional claims in published maps and institutional affiliations.



Copyright: © 2022 by the authors. Licensee MDPI, Basel, Switzerland. This article is an open access article distributed under the terms and conditions of the Creative Commons Attribution (CC BY) license (<https://creativecommons.org/licenses/by/4.0/>).

1. Introduction

Ethanol is an important energy and chemical source, the annual production of which is expected to exceed 130 billion liters worldwide [1]. Compared to the fossil fuels such as ethylene, it is more sustainable to produce bioethanol from renewable biomass. First-generation bioethanol is produced from high-quality food-based feedstocks featuring starch (e.g., potato, and corn) and/or sugar (e.g., sugar cane, and sugar beet), whereas second-generation bioethanol is derived from lignocellulosic biomass [2]. In both cases, the processes involve pretreatment (or fractionation), hydrolysis to sugars (not required for sugar cane), and alcoholic fermentation of sugars [3]. Typical pretreatments include physical (e.g., milling, ultrasonication, steam explosion) [4] and chemical (e.g., dilute acid [5], organosolv [6,7] and hydrotrope [8,9] solvent treatments, as well as reductive fractionation [10,11]) processes. The obtained carbohydrate pulp or extracted starch (or sugars) are ideal sources for industrial-scale production of bioethanol via enzymatic saccharification followed by fermentation. For instance, with the high-quality biomass inputs, little pretreatment (milling and/or sugar extraction) is required to afford relatively high bioethanol yields of 70–75, 400 and 430 L/t from sugar cane, maize, and rice (first-generation biomass sources), respectively [12,13]. The conversion of corn stover, sugarcane bagasse, mixed papers, and poplar (second-generation biomass sources) after delignification (fractionation) can also give various bioethanol yields of 362–456, 318–500, 439, and 419–456 L/t, respectively [13–15].

For the consideration of food safety and the availability of feedstocks, production of ethanol from abundant lignocellulosic biomass has been intensively studied worldwide for years [16]. In general, ethanol is produced via fermentation of glucose that can be

derived from starch, sucrose, and cellulose. The technology for production of ethanol from food-based feedstocks such as starch and sucrose is quite mature, while production of ethanol from lignocellulosic biomass still has some issues [17]. First, glucose is required to release from lignocellulosic biomass for fermentation but this process requires energy-intensive pretreatments and costly cellulolytic enzymes; in addition, enzymatic hydrolysis of cellulose and fermentation of glucose to ethanol take days, so it is necessary to shorten the processing time and increase processing efficiency. Second, enzymes are sensitive to temperature; high temperature cannot be used to accelerate the enzymatic hydrolysis rate because it will inhibit the activity of enzymes and even denature enzymes [18,19]. Despite the fact that acid catalysts (e.g., traditional mineral acids and solid acid catalysts) are also widely studied for cellulose hydrolysis, acid-catalyzed cellulose hydrolysis can lead to further degradation of glucose (e.g., 5-hydroxymethylfurfural (HMF) formation via dehydration) due to the unselective catalytic activity [20–23]. Further studies should be dedicated to developing novel catalysts to improve the yield and selectivity of glucose during cellulose hydrolysis with low cost, as well as developing effective technologies for the post-treatment of cellulose hydrolysate to be compatible with the yeasts. Third, the theoretical yield of ethanol resulting from glucose fermentation is limited to 67%, due to the loss of carbon as CO_2 for the metabolic need of yeasts [17]. Fourth, yeasts are very sensitive to ethanol concentration; high ethanol concentrations will restrict the activity of yeasts. To overcome these issues of the biological process, chemocatalytic conversion of biomass-derived carbohydrates (polysaccharides or monosaccharides) and syngas to ethanol is receiving increasing attention. A chemocatalytic method allows the production of ethanol in higher yields without deactivating the catalyst [24] and avoids the long fermentation cycle and carbon loss related to the biological process (Figure 1) [25]. Therefore, this review mainly introduces the progress in chemocatalytic production of ethanol from lignocellulosic biomass. We analyze the mechanisms of these methods and discuss the issues and prospects associated with these methods.

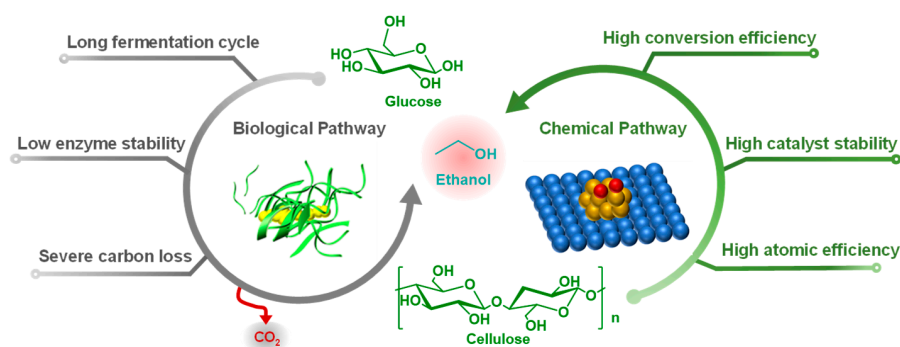


Figure 1. The production of ethanol via biological and chemical pathways.

2. Chemocatalytic Conversion of Biomass-Derived Carbohydrates to Ethanol

Generally, chemical conversion of cellulose (the major carbohydrate component of lignocellulose) to ethanol undergoes the hydrolysis of cellulose to glucose (or its derivatives) and the retro-aldol reaction of glucose to a two-carbon intermediate, glycolaldehyde, which is subsequently hydrogenated to ethanol. Glycolaldehyde (GA) is very active and easy to undergo aldol condensation with itself or other saccharides to form byproducts, reducing the ethanol yield [26]. Due to the instability of glycolaldehyde, current chemocatalytic methods center on maximizing the production of glycolaldehyde for the subsequent hydrogenation process. Based on the production mechanism of glycolaldehyde, chemocatalytic methods can be categorized into one-step and two-step processes.

2.1. Two-Step Process

The W-containing compounds have been considered as the highly active and selective catalysts for glycolaldehyde formation via C–C cleavage of cellulose especially at an ele-

vated temperature ($>200\text{ }^{\circ}\text{C}$) [27]. To stabilize the formed glycolaldehyde, Zhang et al. [28] conducted the retro-aldol reaction of cellulose with the $\text{WO}_x + \text{CMK-3}$ (a physical mixture of WO_x and CMK-3) catalyst in an oxygen atmosphere at $240\text{ }^{\circ}\text{C}$ for 2 h, where glycolaldehyde could undergo readily oxidation upon its formation followed by esterification with methanol to form methyl glycolate (MG) with a yield of up to 57.7 C% (Figure 2a). By following the same conditions (1 MPa O_2 , $240\text{ }^{\circ}\text{C}$, and 2 h), the supported $\text{W}_2\text{C}/\text{CMK-3}$ catalyst could also give high MG yields of 35.5 and 49.1 C% from glucose and Birch, respectively [28]. Due to the superior activity of Cu-based catalyst for the C–O bond hydrogenation compared to the C–C bond hydrogenolysis [29], MG was further hydrogenated under 3 MPa H_2 , and $280\text{ }^{\circ}\text{C}$ with Cu/SiO_2 as a catalyst (Cu nanoparticles with 2–3 nm size were highly dispersed on SiO_2 support) to make ethanol (Figure 2b; Table 1, entry 1). An ethanol yield of 29 C% with a selectivity of 50% was achieved [28].

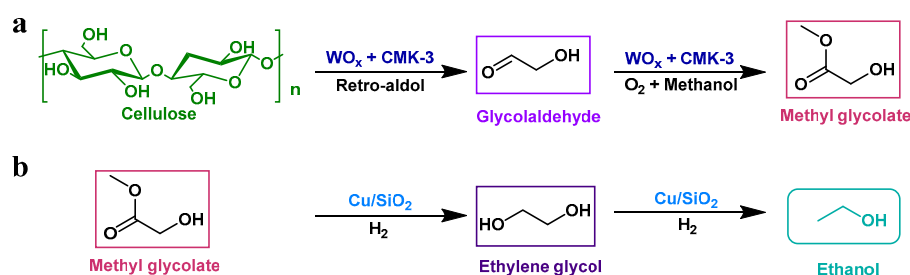


Figure 2. The two-step process towards chemocatalytic conversion of cellulose into ethanol. (a) The formation of intermediate MG from cellulose; (b) the conversion of MG into ethanol via hydrogenation.

Table 1. Chemocatalytic conversion of biomass-derived carbohydrates to ethanol.

En.	Substrate	Substrate Loading, wt%	Solvent/Catalyst	Catalyst Loading, wt%	P(H_2), Mpa	Reaction Temperature, $^{\circ}\text{C}/\text{Time, h}$	Ethanol Yields, C%	Ref.
1	MG	10	THF, Cu/SiO_2	10	3	280	29.0	[28]
2	MG	10	Methanol, 0.1 Pt-Cu/ SiO_2	10	3	230	76.7	[30]
3	MG	10	Methanol, Cu/SiO_2	10	3	230	23.1	[30]
4	Cellulose	1	H_2O , $\text{H}_2\text{WO}_4\text{-Pt}/\text{ZrO}_2$,	0.25/0.5	4	230/5	32.0	[31]
5	Cellulose	1.5	H_2O , 0.1Mo/2Pt/ WO_x	1	6	265/2	43.2	[32]
6	Cellulose	10	H_2O , 0.1Mo/2Pt/ WO_x	1	6	245/2	25.6	[32]
7	Cornstalk	1.5	H_2O , 0.1Mo/2Pt/ WO_x	1	6	245/2	25.5	[32]
8	Miscanthus	1.5	H_2O , 0.1Mo/2Pt/ WO_x	1	6	245/2	26.3	[32]
9	Birch	1.5	H_2O , 0.1Mo/2Pt/ WO_x	1	6	245/2	29.0	[32]
10	Alkaline-pretreated miscanthus	1.5	H_2O , 0.1Mo/2Pt/ WO_x	1	6	245/2	41.3	[32]
11	Cellulose	1	H_2O , 5Ru-25 $\text{WO}_x/\text{HZSM-5}$	1	3	235/20	76.8	[33]
12	Cellulose	1	H_2O , 5Ru-25 $\text{WO}_x/\text{HZSM-5}$ + 5Ru/ WO_x	1/1	3	235/20	87.5	[33]
13	Cellulose	1	0.06 M H_3PO_4 aqueous solution, Ni@C-700	0.375	5.5	200/3	69.1	[34]
14	Cellobiose	1	0.06 M H_3PO_4 aqueous solution, Ni@C-700	0.375	5.5	200/3	39.6	[34]
15	Glucose	1	0.06 M H_3PO_4 aqueous solution, Ni@C-700	0.375	5.5	200/3	35.4	[34]

To selectively obtain the intermediate MG, the generation rate of glycolaldehyde should be comparable to the consumption rate of glycolaldehyde to MG in order to avoid

the accumulation and condensation of glycolaldehyde. In this process, O_2 was used to manipulate the kinetics of the reaction process. In the presence of O_2 , no (hemi)acetal products of glycolaldehyde were detected, which indicated O_2 suppressed the (hemi)acetalization of glycolaldehyde via oxidizing the unstable hemiacetal intermediate products into stable compounds such as MG [35]. By further studying the reaction kinetics over WO_x catalyst in N_2 and O_2 , Zhang et al. [28] observed that the formation rate of MG from cellulose under O_2 atmosphere ($7.7 \text{ mmol mol}_W^{-1} \text{ s}^{-1}$) was two orders of magnitude faster than that of the reaction under N_2 atmosphere ($0.07 \text{ mmol mol}_W^{-1} \text{ s}^{-1}$). In addition, a lower reaction temperature or the presence of water in methanol reduced the yield of MG, but the authors did not explain the specific reasons for the effect of these factors on the catalytic system. According to the formation mechanism of products [36], we speculated that the change in these factors could facilitate the isomerization of glucose to fructose which subsequently underwent another retro-aldol reaction pathway to form glycolaldehyde and dihydroxyacetone, and further to lactic acid and acetic acid. Although methanol as a solvent in this system could effectively improve the hydrothermal stability of the catalyst, methanol could be problematic at large-scale implementation due to its toxicity and volatility. Furthermore, the purification and separation of the intermediate MG may be energy-intensive.

Zhang et al. [30] believed that side reactions during the conversion of cellulose to MG was inevitable while the yield of ethanol from MG could be further improved by optimizing the catalyst system. In order to obtain higher ethanol yield, they developed a novel composite catalyst, Pt-Cu/SiO₂. In this catalyst, Pt and Cu formed a special single-atom alloy (SAA) structure where Pt atoms were completely isolated by surrounding Cu atoms. The SAA structure could also promote the dispersion of Cu atoms, which gave the catalyst a larger specific surface area and better catalytic efficiency than Cu/SiO₂ catalyst without SAA structure [30]. In addition, Pt effectively improved the yield of ethanol by activating H₂ and inhibiting C-C bond cleavage. With the 0.1Pt-Cu/SiO₂ catalyst (Table 1, entry 2), the yield of ethanol from MG reached up to 76.7 C% at 230 °C which was higher than that of the Cu/SiO₂ catalyst (the yield was 23.1 C% at 250 °C; Table 1, entry 3). Also, the catalyst did not lose activity during 700-h operation. The proposed reaction pathways were shown in Figure 3.

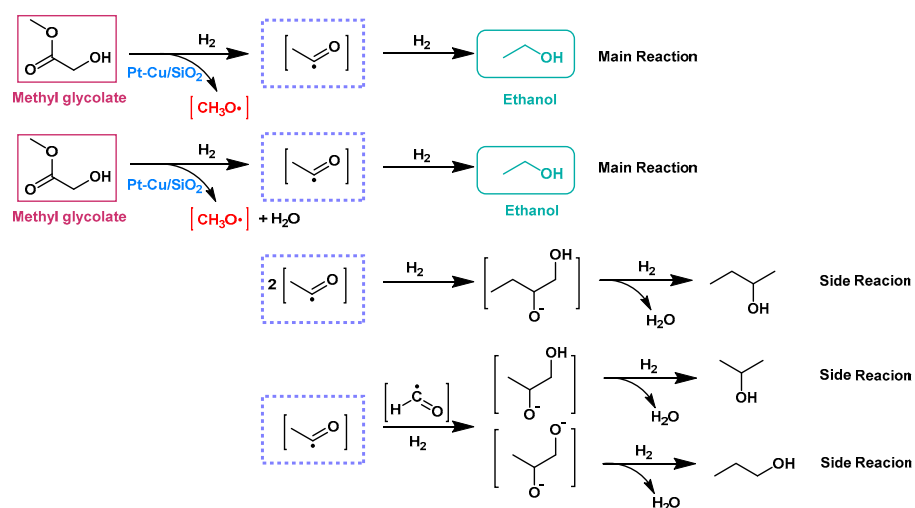


Figure 3. The proposed reaction pathways for MG hydrogenation with Pt-Cu/SiO₂ as a catalyst.

In summary, the two-step processes involve multiple catalysts and intermediates, which could be inefficient and energy-intensive. Therefore, the processes that can convert cellulose to ethanol in one pot were also studied.

2.2. One-Pot Approach

Differently from the two-step process, the one-pot approach can stabilize the unstable intermediate glycolaldehyde via hydrogenation. When glycolaldehyde was generated via the retro-aldol reaction of glucose under an acidic [31] or alkaline [37] condition, it was readily hydrogenated to a stable intermediate, ethylene glycol (EG). However, in such a hydrogenation environment, glucose could be hydrogenated to sorbitol, which was unable to undergo the retro-aldol reaction to form glycolaldehyde due to the lack of a carbonyl group; therefore, it was important to prepare a suitable bifunctional catalyst that could readily catalyze the retro-aldol reaction of glucose to avoid the hydrogenation of glucose to sorbitol and, meanwhile, selectively convert the formed glycolaldehyde to EG. Wang et al. [31] reported a novel one-pot method for direct conversion of cellulose into ethanol in an aqueous medium with $\text{H}_2\text{WO}_4\text{-Pt/ZrO}_2$ as a catalyst (Table 1, entry 4). The highest ethanol yield of 32 C% was achieved from cellulose under 4 MPa H_2 and 250 °C for 5 h, together with the formation of EG, propanol, 1,2-propanediol and alkanes (a total carbon balance of 89–96%). In the presence of H_2WO_4 , only Pt/ZrO₂ achieved high yields of ethanol while other ZrO₂-supported metals (e.g., Ru/ZrO₂, Pd/ZrO₂, Rh/ZrO₂) resulted in the ethanol yields of less than 15 C% [31]. The high activity of Pt could readily catalyze the hydrogenation of GA to EG to avoid the condensation of GA while other metals on ZrO₂ had lower activity to achieve such a purpose. Additionally, when metal oxides with strong acids or weak bases (such as Al₂O₃ and MgO) were used, more C3 alcohols (such as 1,2-propanediol, propanol and glycerol) were generated. The authors believed that Lewis acid and base were more conducive to the conversion of cellulose and/or its derivatives to C3 compounds through isomerization and retro-aldol reactions. When water-soluble carbohydrates such as glucose, cellobiose, and starch were used as the feedstocks, the EG and ethanol yields were lower than that of cellulose under this catalytic condition. The reason was that the hydrolysis of cellulose was a slow process, but the above-mentioned raw materials had high reactivity under this system and were prone to cause more side reactions. For example, sorbitol, the hydrogenation product of glucose, could be hardly converted to ethanol because it was unable to undergo retro-aldol reactions due to the loss of the aldehyde group; fructose, the isomer of glucose, would form C3 retro-aldol intermediates such as glyceraldehyde and dihydroxyacetone and several derivatives such as lactic acid, glycerol, and propanol. These results could be explained by the possible mechanism shown in Figure 4.

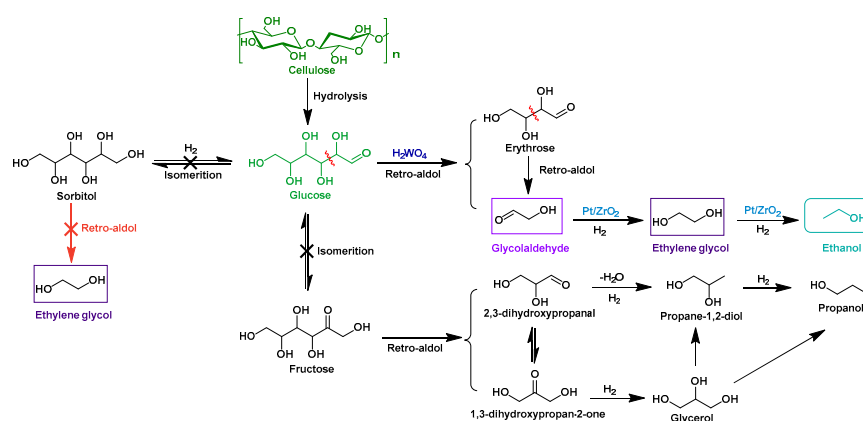


Figure 4. The proposed mechanism for conversion of cellulose into ethanol in one pot with $\text{H}_2\text{WO}_4\text{-Pt/ZrO}_2$ as a catalyst.

A similar catalyst, Mo/Pt/WO_x , could convert cellulose to ethanol in one pot with the yield of 43.2 C% at 265 °C for 2 h (Table 1, entry 5) [32]. WO_x as a Lewis acid catalyzed the retro-aldol cleavage of glucose to form glycolaldehyde, and Mo/Pt/WO_x catalyzed the hydrogenation of glycolaldehyde to EG and ethanol. In the above two-step reaction,

the C–O bond breakage caused by the hydrogenation of EG determined the over-all yield of ethanol because the ethanol yield closely coincided with the Mo content. Besides, the deposition order of Pt and Mo had a substantial effect on the catalytic activity of the resulting catalysts. Deposition of Pt followed by Mo forming a unique structure showed the highest catalytic efficiency. The yield of ethanol decreased from 43.2 to 25.6 C% when cellulose concentration was increased from 1.5 to 10 wt% (Table 1, entry 6), which indicated this catalytic system was not suitable for the catalytic conversion of higher concentrations of cellulose. Zhao et al. [38] deemed that the decrease in the yield of ethanol at higher cellulose concentrations was caused by the cleavage of glucose, an intermediate formed and accumulated during cellulose conversion, not the cleavage of the C–O bond of EG. When the catalytic system was used to catalyze lignocellulosic materials such as cornstalk, miscanthus, and birch, the yields were 25.5, 26.3, and 29.0 C%, respectively (Table 1, entry 7–9) [32]. After removing lignin from these materials by pretreatments, the conversion of these materials was significantly improved (Table 1, entry 10), indicating that lignin has a substantially negative effect on this catalytic system [32].

In addition, Ma et al. [33] reported a novel multifunctional catalyst Ru-WO_x/HZSM-5 with suitable acidity for conversion of cellulose and hemicelluloses to ethanol. As shown in Figure 5, WO_x played an important role in the cleavage of the C–C bonds of glucose units and WO_x promoted the dispersion of Ru and formed Ru₃W₁₇ alloy with W. Ru₃W₁₇ alloy improved the ethanol yield by promoting the hydrogenation of EG. After a 20-h reaction at 235 °C with 3 MPa H₂, the yield of ethanol for 1 wt% of cellulose could reach 76.8 C% (Table 1, entry 11). However, when glucose was used as the substrate under the same conditions, severe carbon loss occurred possibly due to oligomerization of high-concentration glucose and the formation of humins, which were catalyzed by the acid sites of the catalysts. The catalytic system was also very sensitive to the concentration of cellulose. When the cellulose concentration was increased from 1 wt% to 5 wt%, the yield of ethanol yield decreased from 76.8% to 42.3%. The authors concluded that the retro-aldol reaction of glucose was a slow reaction while the side reactions such as oligomerization and dehydration of glucose were faster, thereby resulting in lower ethanol selectivity and yields [33]. The addition of extra Ru/WO_x catalyst, which could promote retro-aldol and hydrogenation reactions, led to higher ethanol yields (the yield for 1 wt% (Table 1, entry 12) and 5 wt% of cellulose was 87.5% and 48.5%, respectively). Moreover, HZSM-5 showed poor hydrothermal stability, which makes it necessary to search for a support with higher hydrothermal stability in the future.

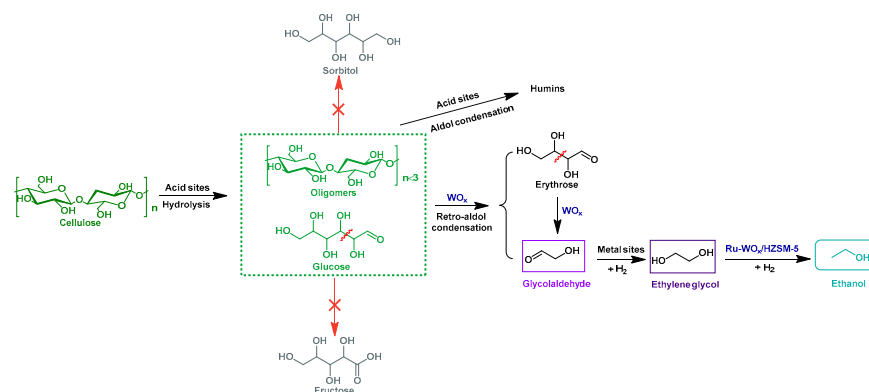


Figure 5. The proposed mechanism for conversion of cellulose to ethanol in one pot with Ru-WO_x/HZSM-5 as a catalyst.

In contrast, graphene-encapsulated nickel (Ni@C) exhibited excellent long-term stability for ethanol production due to the protection of graphene shell [34]. Combined with phosphoric acid and H₂, Ni@C led to an ethanol yield to 69.1% when the concentration of cellulose was 10 g/L (Table 1, entry 13), reaching the theoretical yield of ethanol produced

by fermentation [17,34]. In this catalytic system, phosphoric acid played the role of catalyzing the hydrolysis of cellulose to glucose and forming a cyclic diester intermediate with glucose. The C–O and C–C bonds of the cyclic diester intermediate were selectively broken to form ethanol efficiently. In the repetitive utilization test of the catalyst, the yields were almost the same without Ni leaching in eight cycles, which indicated that the encapsulation of graphene could resist the corrosion of phosphoric acid to Ni and the catalyst still retain the high catalytic activity in the harsh acidic environment. The less graphene carbon layers, the faster the electron migration from the metal to the graphene surface. As a result, the smaller-size Ni particles and the less graphene layers in the catalyst were favorable to improving the activity and catalytic efficiency of the catalyst and the formation of ethanol. The catalytic system could also catalyze cellobiose (Table 1, entry 14) and glucose (Table 1, entry 15) to ethanol with yields of 39.6 C% and 35.4 C% et, respectively [34], which were lower than that of cellulose. When glucose and cellobiose were used as substrates, the concentrations of glucose and cellobiose in the system were higher than that of cellulose, which resulted in more and severer side reactions such as oligomerization and dehydration. In contrast, when cellulose was used as a substrate, glucose formed from slow hydrolysis of cellulose could be readily and selectively converted into ethanol with no accumulation.

3. Conversion of Biomass-Derived Syngas to Ethanol

Syngas (H_2/CO) is generally resulted from gasification of coal or biomass in industry, which can be used for chemical and energy supply through different chemical processes. Currently, direct ethanol synthesis from biomass-derived syngas is one of the most attractive and challenging processes [39,40]. However, this reaction involves some complex processes such as the dissociation of H_2 (H–H cleavage), the generation of intermediates and the coupling between intermediates. Therefore, it seems relatively difficult to achieve one-step synthesis of ethanol from syngas, but cascade catalytic reactions have been widely investigated for ethanol synthesis.

3.1. Multi-Step Processes

The multi-step processes for ethanol synthesis mainly include two pathways (Figure 6). Route A involves syngas to methanol, carbonylation of methanol with CO, and acetic acid (AA) hydrogenation to ethanol. Route B involves syngas to dimethyl ether (DME), carbonylation of DME with CO, and methyl acetate (MA) hydrogenation to ethanol [41–43].

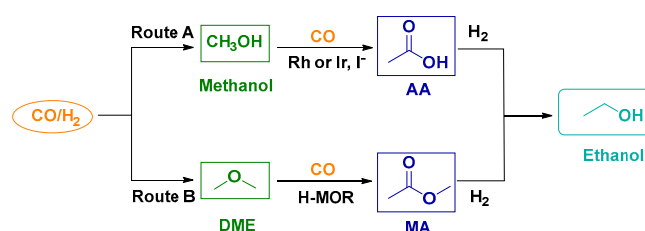


Figure 6. Scheme for ethanol formation via common multi-step reactions.

Previously, Zhou et al. [44] reported a relay catalysis system which enabled the selective conversion of syngas into C_{2+} oxygenates including MA, DME, and ethanol. In such system, several catalysts with different functions were applied in one reactor to synergistically catalyze the conversion of syngas. For instance, the Cu–Zn–Al/H-ZSM-5 catalyst (a mixture of Cu–Zn–Al oxide and H-ZSM-5 powders) could give a high DME selectivity of 93% from syngas at 200 °C for 5 h while a high CH_3OH selectivity was achieved with the use of Cu–Zn–Al oxide solely under the same condition, confirming that H-ZSM-5 could catalyze the dehydration of CH_3OH to DME (Figure 7a) [44,45]. Furthermore, the combination of Cu–Zn–Al/H-ZSM-5 and H-MOR (a weight ratio of 0.5:1) showed a high MA selectivity of 84% together with 13% AA selectivity and a negligible DME selectivity, suggesting that H-MOR functioned for the carbonylation of DME with CO. Therefore, an increased

weight ratio of H-MOR to Cu-Zn-Al/H-ZSM-5 (>0.5:1) could facilitate the formation of MA from syngas [44]. As mentioned before, water released from the formed CH₃OH over the H-ZSM-5 catalyst could also inhibit the followed DME carbonylation via the Cu-Zn-Al oxide-catalyzed water-gas shift (WGS) reaction (i.e., CO + H₂O → CO₂ + H₂). Although most of the H₂O could be removed by the WGS reaction over the combination of Cu-Zn-Al oxide and H-ZSM-5 in direct contact, the small amount of the residual water could lead to the formation of AA, which was unable to form via the DME carbonylation path over H-MOR (Figure 7b) [44,46,47]. The authors also claimed that syngas could be converted into ethanol via DME and MA intermediates in the relay catalysis system. An ethanol selectivity of 52% could be achieved at 6% CO conversion with ZnAl₂O₄ | H-MOR | ZnAl₂O₄ (a sandwich structure) as the catalyst (Figure 7c, Table 2) [44], which was better than most of the reported results for the direct conversion of syngas (Table 2, entry 1–4) [48–51]. Limited by the selectivity of MA and AA during the conversion of syngas over ZnAl₂O₄ | H-MOR, the maximum ethanol selectivity was 64% [44]. These results suggested that the ZnAl₂O₄ in the downstream of the sandwich structure functioned for the hydrogenation of MA and AA intermediates into ethanol.

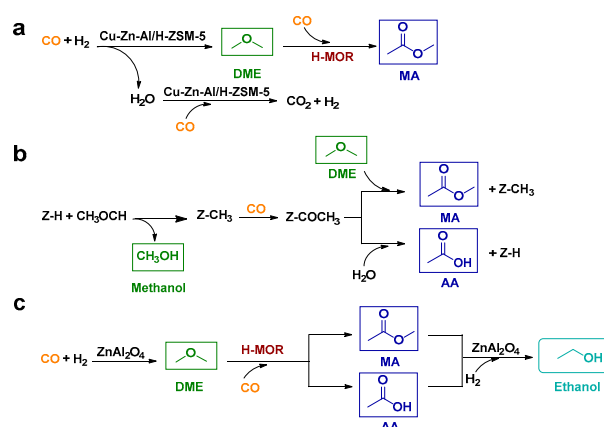


Figure 7. (a) Cu-Zn-Al/H-ZSM-5-catalyzed synthesis of MA from syngas; (b) a possible reaction pathway for formation of AA; (c) ZnAl₂O₄ | H-MOR | ZnAl₂O₄ combination-catalyzed synthesis of ethanol from syngas.

Table 2. Chemocatalytic conversion of biomass-derived syngas to ethanol.

En.	Catalyst	T, °C	P, MPa	H ₂ /CO	WHSV	CO Conv.	Selectivity, %	Ref.
1	7Rh/NFe ₂ O ₃	240	0.1	0.5	1140 h ⁻¹	2.0	27.3	[48]
2	K(C) ₀₆ C ₀₀₅ MoAl ₁₀₀₀	260	7.0	1.0	5000 h ⁻¹	4.4	31.6	[49]
3	Ni ₁ Mo ₁ K _{0.05} -Ni/CNTs	285	5.0	1.0	3000 mL _{STP} h ⁻¹ g ⁻¹	15.5	23.4	[50]
4	CuZnAlOOH	250	4.5	2.0	150 mL/min	3.63	55.5	[51]
5	K ⁺ -ZnO-ZrO ₂ H-MOR-DA-12MR Pt-Sn/SiC	270	5.0	1.0	25 mL min ⁻¹	3.9	90.0	[52]
6	NF-MOR&CZ/SiO ₂	220	1.5	2.0	20 mL/min	-	54.9	[53]
7	1.0%Rh/(5.0%FeO _x -SiO ₂)	250	2.0	2.0	8000 mL g(cat) ⁻¹ h ⁻¹	6.1	45.0	[54]
8	2.5Rh4Fe0.5Li/γ-Al ₂ O ₃	260	2.0	2.0	3600 mL/(g·h)	10.5	30.2	[55]
9	Rh/Ce _{0.8} Zr _{0.2} O ₂	275	2.4	2.0	W/F = 10 g h mol ⁻¹	27.3	25.2	[56]
10	RhMn in CNTs	320	3.0	2.0	12,000 h ⁻¹	8.3	40.0	[57]
11	Rh	270	3.0	2.0	4000 h ⁻¹	5.0	8.2	[58]
12	1.5Rh-0.4Mn/SiO ₂	270	3.0	2.0	4000 h ⁻¹	17	17.7	[58]
13	1.5Rh-4Mn/SiO ₂	270	3.0	2.0	4000 h ⁻¹	5.8	17.7	[58]
14	Rh Mn /SiO ₂	265	5.4	2.0	1700 h ⁻¹	25.1	61.4	[59]
15	RhMn@S-1	320	3.0	2.0	30 mL min ⁻¹	42.4	67.8	[60]
16	Cu ₂ Co ₁ Al	270	2.5	2.0	7500 h ⁻¹	29.2	34.3	[61]
17	CoFe-300	280	3.0	2.0	10,800 mL (g _{cat} h) ⁻¹	52.2	35.0	[62]

In order to reduce the ethanol loss in multiple reactions, Kang et al. [52] designed a triple tandem catalytic system to convert syngas into ethanol with high selectivity. Three catalyst components including K⁺-ZnO-ZrO₂, H-MOR-DA-12MR, and Pt-Sn/SiC were

involved in the tandem system, which catalyzed syngas to CH_3OH , CH_3OH carbonylation to acetic acid (AA), and hydrogenation of AA to ethanol, respectively (Figure 8). The authors claimed that the interplay among the three steps and the compatibility of different catalysts in the syngas stream were crucial to achieve high ethanol selectivity [52]. Specifically, the apparent activation energies for CH_3OH formation, CH_3OH carbonylation, and AA hydrogenation were 81, 71, and 45 kJ mol^{-1} , respectively. The rate of CH_3OH formation (rate-determining step) was the lowest among the three steps in the temperature range of 240–320 °C, which determined the followed carbonylation of CH_3OH with CO. Thus, an elevated temperature facilitated CH_3OH formation, thereby enabling a higher CO conversion over the different catalysts (Table 2), and a relatively high ratio of CO/ CH_3OH was necessary for efficient CH_3OH carbonylation. Furthermore, an increased H_2/CO ratio (from 0.25:1 to 1:1) favored the conversion of CO (an increase from 3.2 to 5.7%) but was unbeneficial to the ethanol selectivity (a slight decrease from 75 to 70%). The existence of H_2 could deactivate the activities of zeolites (i.e. H-MOR) for catalyzing the AA formation. As a result, the AA selectivity was significantly decreased when the H_2/CO ratio was increased to >1:1. This could be caused by that a high H_2/CO ratio accelerated the conversion of CO into by-products such as $\text{C}_2\text{--C}_4$ olefins and CO_2 , reducing the selectivity of ethanol or AA. Apart from the H_2/CO ratio, the total pressure of syngas could affect the CO conversion. A low syngas pressure (<0.5 MPa) generally resulted in hydrocarbons (e.g., $\text{C}_2\text{--C}_4$ olefins), while an increased syngas pressure (from 0.5 to 2.0 MPa) could not only enhance CO conversion but also increase the ethanol selectivity from 11 to 76%. By following the optimized reaction conditions (Table 2, entry 5), a high ethanol selectivity of 90.0% could be achieved at 3.9% CO conversion. Therefore, such catalytic system not only achieved the selective conversion of syngas into ethanol but also offered a strategy for controlling reaction selectivity via decoupling a complicated and uncontrollable reaction system into several well-controlled tandem reactions.



Figure 8. Possible reaction pathway for formation of ethanol in a triple tandem catalytic system. Adapted with permission from *Nat. Commun.* **2020**, *11*, 827–838 [52]. Open access.

3.2. One-Pot Processes

Considering that current zeolite catalysts exhibited undesirable efficiency and stability for the carbonylation of DME to MA during ethanol synthesis from syngas, Yao et al. [53] prepared the nano-filamentous MOR zeolite (NF-MOR) catalyst with diameter of around 70 nm by using nanocrystallization technology. Such nano-MOR zeolite had a larger external surface area and more exposed active sites compared to the common MOR zeolite [63,64], showing superior performance in DME carbonylation reaction and one-step ethanol synthesis. Combined with the CZ/ SiO_2 catalyst, the NF-MOR&CZ/ SiO_2 catalyst could achieve a DME conversion rate of 85% and an ethanol selectivity of 54.9% at 220 °C (Table 2, entry 6) [53].

Due to the superior catalytic performance for CO hydrogenation, Rh-based catalysts have attracted much attention towards one-pot approach for ethanol synthesis from syngas. Since Rh is a rare metal, researchers usually implemented three strategies in order to reduce its loading: (i) preparing supported Rh-based catalysts by using the unique porous structures of the supports [54,55]; (ii) preparing highly dispersed Rh-based catalysts to improve their specific surface areas [65]; (iii) modifying the electronic property of Rh via adding different promoters (e.g., Li, Fe, La, V, Co, or Mn) [56]. For example, Pan et al. [57] reported

that the nanotubes containing Rh particles could substantially improve the ethanol production from syngas. Despite the higher accessibility of the outside of the nanotubes to syngas, an improved ethanol formation rate ($30.0 \text{ mol mol}_{\text{Rh}}^{-1} \text{ h}^{-1}$) by more than an order of magnitude could be achieved inside the nanotubes. Compared to pure Rh (Table 2, entry 11), the use of 1.5Rh-0.4Mn/SiO₂ catalysts (Table 2, entry 12) could significantly increase the CO conversion (5.0% vs. 17.0%) and the ethanol selectivity (8.2% vs. 17.7%) [58]. The promoting effects of Mn have been studied for years. It is generally accepted that the presence of Mn could enhance CO dissociation (C-O cleavage) via forming tilted CO at the interface of Rh–MnO_x [66], meanwhile modifying the electronic property of Rh via forming Rh–MnO_x bimetallic catalysts [58,67]. As an electron-withdrawing component, the formed MnO_x could partially oxidize the Rh atoms at the interface, promoting the insertion of CO to form the CH_xCO* species (Figure 9) [58]. However, excessive Mn could also inhibit the activity by blocking the Rh site, leading to a decreased CO conversion of 5.8% (1.5Rh-4.0Mn/SiO₂; Table 2, entry 13). In addition, a high coverage of CO on the surface of Rh–MnO_x catalyst could inhibit the hydrogenation of CH_xCO* species to CH₃CHO via hindering the adsorption and dissociation of H₂, while an increased H₂ coverage facilitated the deep hydrogenation of CH₃CHO to ethanol and the H-assisted CO dissociation to form OH* species. The OH* species together with CH_xCO* species were important sources for AA formation via coupling reactions, which could also undergo the competing reactions with H* species to form H₂O, CH₃CH₂OH or CH₃CHO (Figure 9). Therefore, the addition of an appropriate amount of Mn (Rh/Mn = 1.5:0.4) and a relatively high ratio of H₂/CO (2:1) was critical to achieve high-selective ethanol production in such catalytic system.

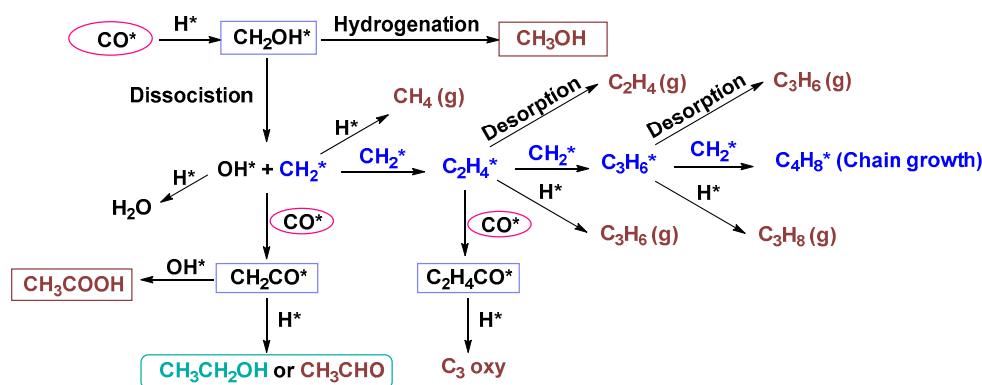


Figure 9. Possible pathways for the formation of hydrocarbon, methanol and C₂₊ oxygenates from CO hydrogenation.

In addition, the catalytic performance of the supported Rh catalysts (Rh-Mn/SiO₂) could be strongly affected by the reaction temperature and pressure. The CO conversion was increased from 24.6% to 40.5% when the reaction temperature was raised from 280 to 300 °C, while ethanol selectivity decreased remarkably from 56.1% to 44.5% and CH₄ selectivity increased from 38.4% to 48.1% [59]. This result suggested that the hydrogenation of CH₂* species to CH₄ was dominant at a higher temperature, which could be explained by the higher activation energy for methanation than for ethanol synthesis. When the total pressure was lowered from 5.4 to 3.8 MPa, CO conversion decreased (from 40.5% to 32.1%), whereas the selectivities of the main products (i.e., ethanol and CH₄) remained almost unchanged under a constant temperature of 300 °C [59], demonstrating that product selectivity was mainly controlled by the reaction temperature rather than the pressure. However, an increased CO conversion was observed with the increased pressure under a relatively lower temperature of 270 °C. It could be because a high pressure facilitated CO insertion into the surface of metal-CH₂* to form C₂ oxygenates, reducing the hydrogenation rate of CH₂* species for CH₄ formation. Therefore, ethanol synthesis over Rh-Mn/SiO₂

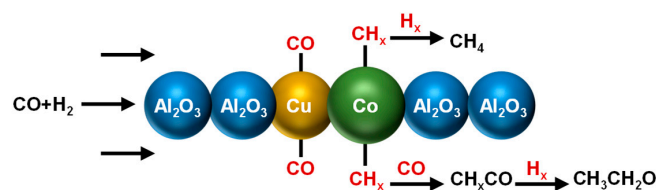


Figure 11. The reaction scheme of CO hydrogenation to ethanol over synergistic catalysis of uniformly dispersed bimetallic CuCo nanosheets.

4. Conclusions and Perspectives

Ethanol, a green energy carrier, has great potential to promote the development of the biorefining industries. However, the production of ethanol via biological pathways has the issues of high cost, long production period, and low atomic economy. The efforts devoted to chemocatalytically converting lignocellulosic biomass to ethanol is effective to reduce processing time and improve atomic economy. Although it is promising, current chemocatalytic pathways also possessed some disadvantages. Chemocatalytic conversion of cellulose to ethanol is mainly achieved through cascade catalytic reactions including cellulose hydrolysis, retro-aldol reaction, and hydrogenation. However, chemocatalytic process also involves some side reactions such as dehydration and aldol condensation. To obtain high-yield ethanol, it is necessary to design multifunctional catalysts which can balance the main and side reactions. Multifunctional and bimetallic catalysts are promising catalysts for the conversion of cellulose to ethanol, but the poor hydrothermal stability of some catalysts or the use of toxic organic solvents limit their large-scale implementations. The future research could be focused on the development of an efficient and green catalytic system that can significantly improve the ethanol yield with reduced cost.

In addition, the synthesis of ethanol from biomass-derived syngas in one or multiple steps is attractive because all components of lignocellulosic biomass including cellulose, hemicelluloses, and lignin could be utilized for ethanol production. DEM, MA and AA are important intermediates in the multi-step conversion of syngas to ethanol. Improving CO conversion and ethanol selectivity is beneficial to obtain high ethanol yield. The adsorption and dissociation of CO with the catalyst, and the ratio of CO/H₂ would affect the ethanol yields resulted from one-step syngas conversion. For one-step conversion of syngas to ethanol, Rh-based catalysts has superior catalytic performance, but of the high cost and scarcity of Rh would limit its wide use. Developing effective non-noble metal catalysts, e.g., transition metal-based bimetallic catalysts, and other multi-functional non-precious metal catalysts, are particularly desired in near future.

Author Contributions: Conceptualization and Funding acquisition, L.S. and X.L. (Xiaolin Luo); writing—original draft preparation, Z.G. and X.L. (Xiaoqing Lv); writing—review and editing, Z.G., X.L. (Xiaoqing Lv), J.Y., X.L. (Xiaolin Luo) and L.S. All authors have read and agreed to the published version of the manuscript.

Funding: This research was funded by National Natural Science Foundation of China (No. 31870559 and 31901262), Outstanding Youth Funding of National Forestry and Grassland Administration (20201326005), Outstanding Youth Funding (xjq201923) of Fujian Agriculture and Forestry University, and Fujian Outstanding Youth Funding (2021J06017).

Data Availability Statement: Data sharing not applicable: No new data were created or analyzed in this study. Data sharing is not applicable to this article.

Acknowledgments: We thank the funding agencies for funding LS's and XL's research NA.

Conflicts of Interest: The authors declare no conflict of interest.

References

1. OECD/FAO. *OECD-FAO Agricultural Outlook 2015-2024*; OECD Publishing: Paris, France, 2015.
2. Jambo, S.A.; Abdulla, R.; Mohd Azhar, S.H.; Marbawi, H.; Gansau, J.A.; Ravindra, P. A review on third generation bioethanol feedstock. *Renew. Sustain. Energy Rev.* **2016**, *65*, 756–769. [[CrossRef](#)]
3. Stephen, J.D.; Mabee, W.E.; Saddler, J.N. Will second-generation ethanol be able to compete with first-generation ethanol? Opportunities for cost reduction. *Biofuels Bioprod. Bioref.* **2012**, *6*, 159–176. [[CrossRef](#)]
4. Aarum, I.; Devle, H.; Ekeberg, D.; Horn, S.J.; Stenström, Y. Characterization of pseudo-lignin from steam exploded birch. *ACS Omega* **2018**, *3*, 4924–4931. [[CrossRef](#)]
5. Sun, Y.; Cheng, J.J. Dilute acid pretreatment of rye straw and bermudagrass for ethanol production. *Bioresour. Technol.* **2005**, *96*, 1599–1606. [[CrossRef](#)]
6. Zhang, K.; Pei, Z.; Wang, D. Organic solvent pretreatment of lignocellulosic biomass for biofuels and biochemicals: A review. *Bioresour. Technol.* **2016**, *199*, 21–33. [[CrossRef](#)] [[PubMed](#)]
7. Liu, J.; Hu, H.; Gong, Z.; Yang, G.; Li, R.; Chen, L.; Huang, L.; Luo, X. Near-complete removal of non-cellulosic components from bamboo by 1-pentanol induced organosolv pretreatment under mild conditions for robust cellulose enzymatic hydrolysis. *Cellulose* **2019**, *26*, 3801–3814. [[CrossRef](#)]
8. Chen, L.; Dou, J.; Ma, Q.; Li, N.; Wu, R.; Bian, H.; Yelle, D.J.; Vuorinen, T.; Fu, S.; Pan, X.; et al. Rapid and near-complete dissolution of wood lignin at ≤ 80 °C by a recyclable acid hydrotrope. *Sci. Adv.* **2017**, *3*, 1–11. [[CrossRef](#)]
9. Luo, X.; Gong, Z.; Shi, J.; Chen, L.; Zhu, W.; Zhou, Y.; Huang, L.; Liu, J. Integrating benzenesulfonic acid pretreatment and bio-based lignin-shielding agent for robust enzymatic conversion of cellulose in bamboo. *Polymers* **2020**, *12*, 191. [[CrossRef](#)]
10. Bosch, S.V.d.; Schutyser, W.; Vanholme, R.; Driessen, T.; Koelewijn, S.; Renders, T.; Meester, B.D.; Huijgen, W.J.J.; Dehaen, W.; Courtin, C.M.; et al. Reductive lignocellulose fractionation into soluble lignin-derived phenolic mono- and dimers and processable carbohydrate pulp. *Energy Environ. Sci.* **2015**, *8*, 1748–1763. [[CrossRef](#)]
11. Liao, Y.; Koelewijn, S.F.; Van den Bossche, G.; Sels, B.F. A sustainable wood biorefinery for low-carbon footprint chemicals production. *Science* **2020**, *367*, 1385–1390. [[CrossRef](#)]
12. *The State of Food and Agriculture 2008. Biofuels: Prospects, Risks and Opportunities*; FAO Publishing: Rome, Italy, 2008. Available online: <http://www.fao.org/3/i0100e/i0100e.pdf> (accessed on 5 August 2021).
13. Tse, T.J.; Wiens, D.J.; Reaney, M.J.T. Production of bioethanol—A review of factors affecting ethanol yield. *Fermentation* **2021**, *7*, 268. [[CrossRef](#)]
14. Corbin, K.R.; Byrt, C.S.; Bauer, S.; DeBolt, S.; Chambers, D.; Holtum, J.A.; Karem, G.; Henderson, M.; Lahnstein, J.; Beahan, C.T.; et al. Prospecting for energy-rich renewable raw materials: Agave leaf case study. *PLoS One* **2015**, *10*, 1–23. [[CrossRef](#)]
15. Nwakaire, J.N.; Ezeoha, S.L.; Ugwuishiwu, B.O. Production of cellulosic ethanol from wood sawdust. *Agric. Eng. Int. CIGR J.* **2013**, *15*, 136–140.
16. Arifin, Y.; Tanudjaja, E.; Dimiyati, A.; Pinontoan, R. A second generation biofuel from cellulosic agricultural by-product fermentation using clostridium species for electricity generation. *Energy Procedia* **2014**, *47*, 310–315. [[CrossRef](#)]
17. Kennes, D.; Abubackar, H.N.; Diaz, M.; Veiga, M.C.; Kennes, C. Bioethanol production from biomass: Carbohydrate vs syngas fermentation. *J. Chem. Technol. Biotechnol.* **2016**, *91*, 304–317. [[CrossRef](#)]
18. Palmqvist, E.; Hägerdal, B.H. Fermentation of lignocellulosic hydrolysates. II: Inhibitors and mechanisms of inhibition. *Bioresour. Technol.* **2000**, *74*, 25–33. [[CrossRef](#)]
19. Modig, T.; Lidén, G.; Taherzadeh, M.J. Inhibition effects of furfural on alcohol dehydrogenase, aldehyde dehydrogenase and pyruvate dehydrogenase. *Biochem. J.* **2002**, *363*, 769–776. [[CrossRef](#)]
20. Palkovits, R.; Tajvidi, K.; Procelewska, J.; Rinaldi, R.; Ruppert, A. Hydrogenolysis of cellulose combining mineral acids and hydrogenation catalysts. *Green Chem.* **2010**, *12*, 972–978. [[CrossRef](#)]
21. Orozco, A.M.; Al-Muhtaseb, A.a.H.; Albadarin, A.B.; Rooney, D.; Walkera, G.M.; Ahmad, M.N.M. Acid-catalyzed hydrolysis of cellulose and cellulosic waste using a microwave reactor system. *Rsc Adv.* **2011**, *1*, 839–846. [[CrossRef](#)]
22. Li, Z.; Fei, B.; Jiang, Z. Comparison of dilute organic and sulfuric acid pretreatment for enzymatic hydrolysis of bamboo. *BioResources* **2014**, *9*, 5652–5661. [[CrossRef](#)]
23. Tarabanko, N.; Baryshnikov, S.V.; Kazachenko, A.S.; Miroshnikova, A.; Skripnikov, A.M.; Lavrenov, A.V.; Taran, O.P.; Kuznetsov, B.N. Hydrothermal hydrolysis of microcrystalline cellulose from birch wood catalyzed by Al₂O₃-B₂O₃ mixed oxides. *Wood Sci. Technol.* **2022**, *56*, 437–457. [[CrossRef](#)]
24. Himmel, M.E.; Ding, S.; Johnson, D.K.; Adney, W.S.; Nimlos, M.R.; Brady, J.W.; Foust, T.D. Biomass recalcitrance: Engineering plants and enzymes for biofuels production. *Science* **2007**, *315*, 804–807. [[CrossRef](#)]
25. Wei, N.; Quarterman, J.; Kim, S.R.; Cate, J.H.D.; Jin, Y. Enhanced biofuel production through coupled acetic acid and xylose consumption by engineered yeast. *Nat. Commun.* **2013**, *4*, 2580–2588. [[CrossRef](#)]
26. Zhang, L.; Wang, W.; Wang, A.; Cui, Y.; Yang, X.; Huang, Y.; Liu, X.; Liu, W.; Son, J.; Oji, H.; et al. Aerobic oxidative coupling of alcohols and amines over Au-Pd/resin in water: Au/Pd molar ratios switch the reaction pathways to amides or imines. *Green Chem.* **2013**, *15*, 2680–2684. [[CrossRef](#)]
27. Liu, Y.; Luo, C.; Liu, H. Tungsten trioxide promoted selective conversion of cellulose into propylene glycol and ethylene glycol on a ruthenium catalyst. *Angew. Chem. Int. Ed.* **2012**, *51*, 3249–3253. [[CrossRef](#)]

28. Xu, G.; Wang, A.; Pang, J.; Zhao, X.; Xu, J.; Lei, N.; Wang, J.; Zheng, M.; Yin, J.; Zhang, T. Chemocatalytic conversion of cellulosic biomass to methyl glycolate, ethylene glycol, and ethanol. *ChemSusChem* **2017**, *10*, 1390–1394. [[CrossRef](#)]
29. Wen, C.; Cui, Y.; Chen, X.; Zong, B.; Dai, W.-L. Reaction temperature controlled selective hydrogenation of dimethyl oxalate to methyl glycolate and ethylene glycol over copper-hydroxyapatite catalysts. *Appl. Catal. B Environ.* **2015**, *162*, 483–493. [[CrossRef](#)]
30. Yang, C.; Miao, Z.; Zhang, F.; Li, L.; Liu, Y.; Wang, A.; Zhang, T. Hydrogenolysis of methyl glycolate to ethanol over a Pt–Cu/SiO₂ single-atom alloy catalyst: A further step from cellulose to ethanol. *Green Chem.* **2018**, *20*, 2142–2150. [[CrossRef](#)]
31. Song, H.; Wang, P.; Li, S.; Deng, W.; Li, Y.; Zhang, Q.; Wang, Y. Direct conversion of cellulose into ethanol catalysed by a combination of tungstic acid and zirconia-supported Pt nanoparticles. *Chem. Commun.* **2019**, *55*, 4303–4306. [[CrossRef](#)]
32. Yang, M.; Qi, H.; Liu, F.; Ren, Y.; Pan, X.; Zhang, L.; Liu, X.; Wang, H.; Pang, J.; Zheng, M.; et al. One-pot production of cellulosic ethanol via tandem catalysis over a multifunctional Mo/Pt/WO_x catalyst. *Joule* **2019**, *3*, 1937–1948. [[CrossRef](#)]
33. Li, C.; Xu, G.; Wang, C.; Ma, L.; Qiao, Y.; Zhang, Y.; Fu, Y. One-pot chemocatalytic transformation of cellulose to ethanol over Ru–WO_x/HZSM-5. *Green Chem.* **2019**, *21*, 2234–2239. [[CrossRef](#)]
34. Liu, Q.; Wang, H.; Xin, H.; Wang, C.; Yan, L.; Wang, Y.; Zhang, Q.; Zhang, X.; Xu, Y.; Huber, G.W.; et al. Selective cellulose hydrogenolysis to ethanol using Ni@C combined with phosphoric acid catalysts. *ChemSusChem* **2019**, *12*, 3977–3987. [[CrossRef](#)]
35. Hayashi, T.; Inagaki, T.; Itayama, N.; Baba, H. Selective oxidation of alcohol over supported gold catalysts: Methyl glycolate formation from ethylene glycol and methanol. *Catal. Today* **2006**, *117*, 210–213. [[CrossRef](#)]
36. Liu, X.; Liu, X.; Xu, G.; Zhang, Y.; Wang, C.; Lu, Q.; Ma, L. Highly efficient catalytic conversion of cellulose into acetol over Ni–Sn supported on nanosilica and the mechanism study. *Green Chem.* **2019**, *21*, 5647–5656. [[CrossRef](#)]
37. Luo, X.; Gong, Z.; Yang, G.; Huang, L.; Chen, L.; Shuai, L. In-situ oxidation/reduction facilitates one-pot conversion of lignocellulosic biomass to bulk chemicals in alkaline solution. *Chem. Eng. J.* **2022**, *429*, 132365. [[CrossRef](#)]
38. Zhao, G.; Zheng, M.; Zhang, J.; Wang, A.; Zhang, T. Catalytic conversion of concentrated glucose to ethylene glycol with semicontinuous reaction system. *Ind. Eng. Chem. Res.* **2013**, *52*, 9566–9572. [[CrossRef](#)]
39. Ciliberti, C.; Biundo, A.; Albergo, R.; Agrimi, G.; Braccio, G.; de Bari, I.; Pisano, I. Syngas derived from lignocellulosic biomass gasification as an alternative resource for innovative bioprocesses. *Processes* **2020**, *8*, 1567. [[CrossRef](#)]
40. Luk, H.T.; Mondelli, C.; Ferre, D.C.; Stewart, J.A.; Perez-Ramirez, J. Status and prospects in higher alcohols synthesis from syngas. *Chem. Soc. Rev.* **2017**, *46*, 1358–1426. [[CrossRef](#)]
41. Climent, M.J.; Corma, A.; Iborra, S.; Sabater, M.J. Heterogeneous catalysis for tandem reactions. *ACS Catal.* **2014**, *4*, 870–891. [[CrossRef](#)]
42. Wang, S.; Yin, S.; Guo, W.; Liu, Y.; Zhu, L.; Wang, X. Influence of inlet gas composition on dimethyl ether carbonylation and the subsequent hydrogenation of methyl acetate in two-stage ethanol synthesis. *New J. Chem.* **2016**, *40*, 6460–6466. [[CrossRef](#)]
43. Zhang, F.; Chen, K.; Jiang, Q.; He, S.; Chen, Q.; Liu, Z.; Kang, J.; Zhang, Q.; Wang, Y. Selective transformation of methanol to ethanol in the presence of syngas over composite catalysts. *ACS Catal.* **2022**, *12*, 8451–8461. [[CrossRef](#)]
44. Zhou, W.; Kang, J.; Cheng, K.; He, S.; Shi, J.; Zhou, C.; Zhang, Q.; Chen, J.; Peng, L.; Chen, M.; et al. Direct conversion of syngas into methyl acetate, ethanol, and ethylene by relay catalysis via the intermediate dimethyl ether. *Angew. Chem. Int. Ed.* **2018**, *57*, 12012–12016. [[CrossRef](#)]
45. Yang, G.; Tsubaki, N.; Shamoto, J.; Yoneyama, Y.; Zhang, Y. Confinement effect and synergistic function of H-ZSM-5/ Cu–ZnO–Al₂O₃ capsule catalyst for one-step controlled synthesis. *J. Am. Chem. Soc.* **2010**, *132*, 8129–8136. [[CrossRef](#)]
46. Cheung, P.; Bhan, A.; Sunley, G.J.; Iglesia, E. Selective carbonylation of dimethyl ether to methyl acetate catalyzed by acidic zeolites. *Angew. Chem. Int. Ed.* **2006**, *45*, 1617–1620. [[CrossRef](#)]
47. Xue, H.; Huang, X.; Ditzel, E.; Zhan, E.; Ma, M.; Shen, W. Dimethyl ether carbonylation to methyl acetate over nanosized mordenites. *Ind. Eng. Chem. Res.* **2013**, *52*, 11510–11515. [[CrossRef](#)]
48. Carrillo, P.; Shi, R.; Teeluck, K.; Senanayake, S.D.; White, M.G. In situ formation of FeRh nanoalloys for oxygenate synthesis. *ACS Catal.* **2018**, *8*, 7279–7286. [[CrossRef](#)]
49. Toyoda, T.; Minami, T.; Qian, E.W. Mixed alcohol synthesis over sulfided molybdenum-based catalysts. *Energy Fuels* **2013**, *27*, 3769–3777. [[CrossRef](#)]
50. Ma, C.H.; Li, H.Y.; Lin, G.D.; Zhang, H.B. Ni-decorated carbon nanotube-promoted Ni–Mo–K catalyst for highly efficient synthesis of higher alcohols from syngas. *Appl. Catal. B Environ.* **2010**, *100*, 245–253. [[CrossRef](#)]
51. Gu, Y.; Han, C.; Huang, J.; Vinokurov, V.A.; Huang, W. CuZnAlOOH catalysts with Cu⁰/Cu⁺ constructed by two-step hydrolysis for ethanol production from syngas. *Fuel* **2022**, *322*, 124111–124121. [[CrossRef](#)]
52. Kang, J.; He, S.; Zhou, W.; Shen, Z.; Li, Y.; Chen, M.; Zhang, Q.; Wang, Y. Single-pass transformation of syngas into ethanol with high selectivity by triple tandem catalysis. *Nat. Commun.* **2020**, *11*, 827–838. [[CrossRef](#)]
53. Yao, J.; Feng, X.; Fan, J.; Komiyama, S.; Kugue, Y.; Guo, X.; He, Y.; Yang, G.; Tsubaki, P.N. Self-assembled nano-filamentous zeolite catalyst to realize efficient one-step ethanol synthesis. *Chem. Eur. J.* **2022**, *1–12*. [[CrossRef](#)] [[PubMed](#)]
54. Wang, J.; Zhang, Q.; Wang, Y. Rh-catalyzed syngas conversion to ethanol: Studies on the promoting effect of FeO_x. *Catal. Today* **2011**, *171*, 257–265. [[CrossRef](#)]
55. Chen, Y.; Zhang, H.; Ma, H.; Qian, W.; Jin, F.; Ying, W. Direct conversion of syngas to ethanol over Rh–Fe/γ–Al₂O₃ catalyst: Promotion effect of Li. *Catal. Lett.* **2018**, *148*, 691–698. [[CrossRef](#)]
56. Liu, Y.; Murata, K.; Inaba, M.; Takahara, I.; Okabe, K. Synthesis of ethanol from syngas over Rh/Ce_{1–x}Zr_xO₂ catalysts. *Catal. Today* **2011**, *164*, 308–314. [[CrossRef](#)]

57. Pan, X.; Fan, Z.; Chen, W.; Ding, Y.; Luo, H.; Bao, X. Enhanced ethanol production inside carbon-nanotube reactors containing catalytic particles. *Nat. Mater.* **2007**, *6*, 507–511. [[CrossRef](#)]
58. Mao, W.; Su, J.; Zhang, Z.; Xu, X.; Dai, W.; Fu, D.; Xu, J.; Zhou, X.; Han, Y. Kinetics study of C₂₊ oxygenates synthesis from syngas over Rh–MnO_x/SiO₂ catalysts. *Chem. Eng. Sci.* **2015**, *135*, 312–322. [[CrossRef](#)]
59. Hu, J.; Wang, Y.; Cao, C.; Elliott, D.C.; Stevens, D.J.; White, J.F. Conversion of biomass-derived syngas to alcohols and C₂ oxygenates using supported Rh catalysts in a microchannel reactor. *Catal. Today* **2007**, *120*, 90–95. [[CrossRef](#)]
60. Wang, C.; Zhang, J.; Qin, G.; Wang, L.; Zuidema, E.; Yang, Q.; Dang, S.; Yang, C.; Xiao, J.; Meng, X.; et al. Direct conversion of syngas to ethanol within zeolite crystals. *Chem* **2020**, *6*, 646–657. [[CrossRef](#)]
61. Sun, K.; Gao, X.; Bai, Y.; Tan, M.; Yang, G.; Tan, Y. Synergetic catalysis of bimetallic copper–cobalt nanosheets for direct synthesis of ethanol and higher alcohols from syngas. *Catal. Sci. Technol.* **2018**, *8*, 3936–3947. [[CrossRef](#)]
62. Zeng, Z.; Li, Z.; Guan, T.; Guo, S.; Hu, Z.; Wang, J.; Rykov, A.; Lv, J.; Huang, S.; Wang, Y.; et al. CoFe alloy carbide catalysts for higher alcohols synthesis from syngas: Evolution of active sites and Na promoting effect. *J. Catal.* **2022**, *405*, 430–444. [[CrossRef](#)]
63. Li, L.; Wang, Q.; Liu, H.; Sun, T.; Fan, D.; Yang, M.; Tian, P.; Liu, Z. Preparation of spherical mordenite zeolite assemblies with excellent catalytic performance for dimethyl ether carbonylation. *ACS Appl. Mater. Interfaces* **2018**, *10*, 32239–32246. [[CrossRef](#)]
64. Ham, H.; Jung, H.S.; Kim, H.S.; Kim, J.; Cho, S.J.; Lee, W.B.; Park, M.-J.; Bae, J.W. Gas-phase carbonylation of dimethyl ether on the stable seed-derived ferrierite. *ACS Catal.* **2020**, *10*, 5135–5146. [[CrossRef](#)]
65. Zhang, Y.; Grass, M.E.; Kuhn, J.N.; Tao, F.; Habas, S.E.; Huang, W.; Yang, P.; Somorjai, G.A. Highly selective synthesis of catalytically active monodisperse rhodium nanocubes. *J. Am. Chem. Soc.* **2008**, *130*, 5868–5869. [[CrossRef](#)]
66. Stevenson, S.A.; Kniiziuger, H. Carbon monoxide hydrogenation on supported Rh–Mn catalysts. *J. Mol. Catal.* **1990**, *63*, 201–211.
67. Ojeda, M.; Granados, M.L.; Rojas, S.; Terreros, P.; García-García, F.J.; Fierro, J.L.G. Manganese-promoted Rh/Al₂O₃ for C₂-oxygenates synthesis from syngas. *Appl. Catal. A Gen.* **2004**, *261*, 47–55. [[CrossRef](#)]
68. Lausche, A.C.; Medford, A.J.; Khan, T.S.; Xu, Y.; Bligaard, T.; Abild-Pedersen, F.; Nørskov, J.K.; Studt, F. On the effect of coverage-dependent adsorbate–adsorbate interactions for CO methanation on transition metal surfaces. *J. Catal.* **2013**, *307*, 275–282. [[CrossRef](#)]
69. Mei, D.; Rousseau, R.; Kathmann, S.M.; Glezakou, V.-A.; Engelhard, M.H.; Jiang, W.; Wang, C.; Gerber, M.A.; White, J.F.; Stevens, D.J. Ethanol synthesis from syngas over Rh-based/SiO₂ catalysts: A combined experimental and theoretical modeling study. *J. Catal.* **2010**, *271*, 325–342. [[CrossRef](#)]
70. Cao, A.; Schumann, J.; Wang, T.; Zhang, L.; Xiao, J.; Bothra, P.; Liu, Y.; Abild-Pedersen, F.; Nørskov, J.K. Mechanistic insights into the synthesis of higher alcohols from syngas on CuCo alloys. *ACS Catal.* **2018**, *8*, 10148–10155. [[CrossRef](#)]